Frontiers of Physics
https://doi.org/10.1007/s11467-019-0893-4
Front. Phys.
14(4), 43401 (2019)

REVIEW ARTICLE

Topological insulator: Spintronics and quantum computations

Mengyun He[1,2], **Huimin Sun**[1,2], **Qing Lin He**[1,2,†]

[1] *International Center for Quantum Materials, School of Physics, Peking University, Beijing 100871, China*
[2] *CAS Center for Excellence in Topological Quantum Computation, University of Chinese Academy of Sciences, Beijing 100190, China*
Corresponding author. E-mail: [†] *qlhe@pku.edu.cn*
Received January 26, 2019; accepted March 8, 2019

Topological insulators are emergent states of quantum matter that are gapped in the bulk with time-reversal symmetry-preserved gapless edge/surface states, adiabatically distinct from conventional materials. By proximity to various magnets and superconductors, topological insulators show novel physics at the interfaces, which give rise to two new areas named topological spintronics and topological quantum computation. Effects in the former such as the spin torques, spin-charge conversion, topological antiferromagnetic spintronics, and skyrmions realized in topological systems will be addressed. In the latter, a superconducting pairing gap leads to a state that supports Majorana fermions states, which may provide a new path for realizing topological quantum computation. Various signatures of Majorana zero modes/edge mode in topological superconductors will be discussed. The review ends by outlooks and potential applications of topological insulators. Topological superconductors that are fabricated using topological insulators with superconductors have a full pairing gap in the bulk and gapless surface states consisting of Majorana fermions. The theory of topological superconductors is reviewed, in close analogy to the theory of topological insulators.

Keywords topological insulator, Majorana fermion, topological spintronics, topological superconductor

Contents

1 Introduction

Topological states of fermionic matter were considered as a paradigm for investigating the ordered states of matter from the perspective of topology, symmetry and the spontaneous breaking counterpart [1, 2]. On one hand, these topological phases are distinct from other trivial phases from non-local order parameters as well as phases transitions denoted by the evolution of the topology. Specifically, this can be signified by the discontinuity of the so-called topological invariant, which describes the topological nature of the system in the momentum space, or counts the number of edge states in real space in some cases. On the other hand, the existence of the topological order usually depends on the emergence or breaking of certain symmetry [3]. Usually, novel topological properties appear when a topological order is present, which exhibit robustness against symmetry-preserving perturbations. This is known as a topological protection [4, 5]. The best known example of a topological phase is the integer quantum Hall state, whose edges can host chiral states and contribute to a quantized Hall conductivity [6, 7]. These edge states arise due to a nontrivial wave function topology that can be measured in terms of a quantized topological invariant, i.e., the Thouless–Kohmoto–Nightingale–den Nijs number or the Chern number in this case [7]. Therefore, the integer quantum Hall insulator is also known as a Chern insulator. Such an invariant is proportional to the Hall conductivity given by the sum of all filled bands in the material's band structure. The system is topologically non-trivial because this invariant remains intact when adiabatic deformations are applied to the system as long as the bulk gap remains open. In recent years, the groundbreaking discovery of a new quantum state of matter, that is, topological insu-

lators (TIs) [8–12], exemplifies such a topological phase of quantum matter, which is characterized by a Z_2 invariant and protected by time-reversal symmetry [13–15]. Due to the topological protection, massless Dirac fermions in the TI surfaces are immune to spin-independent scattering and localization, endowing TIs with promise for exploring fundamental physics, spin-based electronics and fault-tolerant information processing. Tremendous progress in understanding the topological nature, implementing to application, and exploring more topological materials had been made, which gave rise to an upsurge in the area of topological physics. Some new topological phases, like the Dirac/Weyl semimetals [16], topological superconductors [2], and interacting bosonic and fermionic systems were also theoretically predicted and experimentally discovered.

One of the striking features in TIs is the strong intrinsic spin–orbit coupling (SOC). This coupling opens up a bulk band gap and results in an odd number of band inversions, therefore altering the wave function topology of the quantum state [12, 17–19]. This manifests as an odd number of helical edge states and Dirac cone surface states in two- and three-dimensional TIs, respectively. The helical states exhibit an exotic property that the electron's momentum and spin in the TI edges/surfaces are constrained to be perpendicular to each other. Using such a property, a net carrier momentum induced by a bias current can spontaneously generate a net spin polarization at the edges/surfaces of the TIs. Therefore, TIs are regarded as an inherent spin-current generator. Furthermore, in a heterostructure consisting of a TI and a magnet, a charge flow on the TI surfaces can lead to a non-equilibrium surface spin accumulation on account of the spin-momentum locking property [20]. If such a spin accumulation couples to the adjacent magnet, the resulting flow of spin angular momentum can exert a spin-transfer torque onto the magnet. Therefore, the helical locking sheds light on TIs as a potential spin accumulator as well [21]. Besides the intrinsic TIs, in a magnetic TI with chiral edge states, it was also shown that such edge states exhibited a topologically stable spin texture at the boundary when a chiral-like symmetry was present [22]. The edge spin polarization depends on the propagating direction of the edge state and magnetization direction. Based on such a property, a controllable way to generate and filter spin-polarized currents using magnetic TI was proposed [23]. In short, the topological states in TIs enable a high efficient spin-current generator/accumulator/filter owning to their high spin-to-charge (or vice versa) conversion efficiency and allow efficient manipulations to the adjacent magnets and thus spins. Spintronic devices based on TIs enjoy advantages in novel computation, logic, and memory devices applications.

The spin-momentum locking property also enables TIs to host Majorana fermions when superconductivity is induced at the TI edges/surfaces via superconducting proximity effect [2, 24]. Because of such a helical locking effect, the two edge/surface bands in TIs are spin non-degenerate. In this way, the intra-band pairing has to be odd, similar to the unconventional p-wave superconductivity that carries zero-energy Majorana states. This immediately implies that a Majorana fermion can be bounded in the vortex core of this induced superconductor. Such a superconductor is also known as a topological superconductor. The Majorana fermions accommodating in this superconductor obey non-Abelian statistics and therefore are named as non-Abelian anyons, which are believed to revolutionize the quantum computation. One dimension higher than this zero-dimensional Majorana bound state, a one-dimensional Majorana edge state is shown to allow similar non-Abelian quantum operations on electronic states. Both Majorana bound states and edge states exhibit great potential to form qubits for fault-tolerant topological quantum computation [25, 26].

In this review, we will focus on the TI as a typical example of topological phases. Application of the topological properties in areas of spintronics and quantum computation will be present. We review the recent theoretical and experimental progresses on spin-transport using TIs that relate to the topological aspects of spintronics. The development of topological superconductor and Majorana fermion in topological quantum computation will also be addressed.

2 Topological spintronics

When the topology in quantum materials meets spintronics, an emergent area called topological spintronics arises, which focuses on interesting interactions between topological states and the spins of carriers in the adjacent magnets. In this way, spintronic effects such as spin–orbit/-transfer torques, spin pumping, spin current generation and injection, unidirectional spin-Hall effect, as well as the interfacial exchange coupling can be tailored by using different TI/magnet structures and device structures. In the following, the TI will be used as a typical example and its applications in spintronics will be reviewed.

2.1 Spin transfer torque (STT) and spin–orbit torque (SOT) in TIs

Recent studies in heavy metal/magnet heterostructures demonstrate that the dominant mechanism to reorient the magnetization by applying charge current or power is usually attributed to spin torques. The torque originates in the Rashba–Edelstein effect in topologically trivial materials, but this torque effect still holds for topologically nontrivial materials and their heterostructures with magnets [27–31]. As shown in Fig. 1, when a charge current is applied to the surface of a three-dimensional TI, the accumulation of forward-going Dirac electrons overwhelms

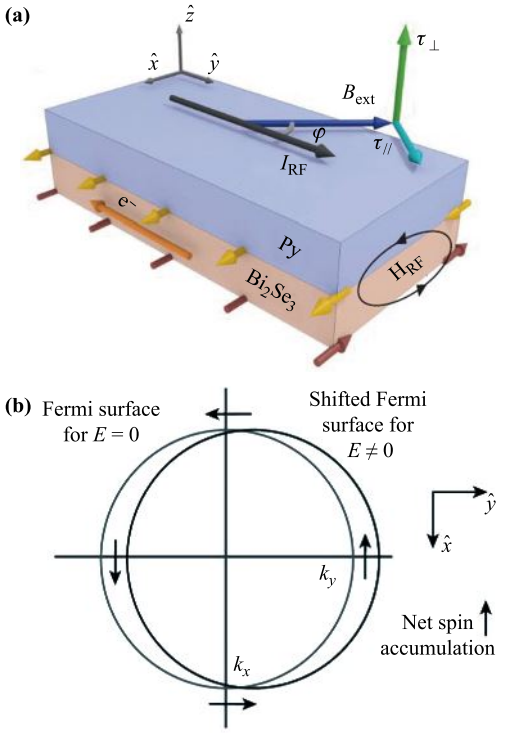

Fig. 1 **(a)** Schematic diagram of the heterostructure and coordinate system. The yellow and red arrows denote spin moment directions. Py, permalloy. **(b)** The mechanism by which an in-plane current in a TI surface state generates a non-equilibrium surface spin accumulation, on account of locking between the spin direction and wavevector for electrons in the surface state. The arrows denote the directions of spin magnetic moments, which are opposite to the corresponding spin angular momenta. Reproduced from Ref. [20].

with those backward-going owing to the helical locking of the electron's spin and momentum [20]. In this way, the flow of the charge current induces a non-equilibrium surface spin current. By coupling to the adjacent magnet, this spin-polarized current can transfer the spin angular momentum to exert an STT on the adjacent magnet. The quantity of the effective spin current conductivity is $\sigma_{S,i} = J_{S,i}/E = \tau_i M_S t/(E\cos\ \varphi)$, where $J_{S,i}$ is the i component (// or $\perp$) of the spin current density absorbed by the magnet for $\varphi = 0°$, E is the amplitude of the electric field, M_S is the saturation magnetization, and t is the thickness of the magnet. It is worth mentioning that this mechanism depends on neither the Fermi level relative to the Dirac point of the TI, nor the bulk conductivity, evidenced by spin torque ferromagnetic resonance experiments. The sign of $\sigma_{S,//}$ is in agreement with the picture for spin transfer from the spin accumulation of the topological surface electrons, resulting in spin moment in direction of $\hat{z}\times\hat{k}$. Here $\hat{z}$ is the surface normal and $\hat{k}$ is the electron wavevector direction. The corresponding accumulation of spin angular momentum hence lies in the direction of $-\hat{z}\times\hat{k}$. Even the sign of the out-of-plane spin current conductivity, $\sigma_{S,\perp}$, is the same as that of the torque due to an Oersted field, but this is excluded since the resulting magnitude is much greater than that expected in the Oersted field. Importantly, the values of both in-plane and out-of-plane spin current conductivities are comparable to those for the most efficient spin current sources in heavy metal cases, which generate current-induced spin currents by the spin Hall effect. However, because the electrical conductivities of the heavy metals are much greater than those of the TI, it indicates that the resulting strength of STT per unit current is greater in TI when compared with that of the heavy metals.

If the role of the polarizer in the above STT picture is replaced by the SOC of the material, i.e., the spin-polarized current is generated by the bulk spin Hall effect of the SOC material or the interfacial spin–orbit interaction in a heterostructure, the spin angular momentum can also be transferred into the adjacent magnet. Hence, such a torque is named as SOT, emphasizing the role played by the SOC. Likewise, due to the helical locking and strong SOC in TIs, the SOT should also exist in the TI/magnet heterostructure required by both the spin Hall effect from bulk states together with inverse spin galvanic and magnetoelectric effects at the interface. Importantly, in this heterostructure, the helical locking of the topological surface states account for the spin accumulation with a different sign and a much larger magnitude compared with those produced in topologically trivial materials. Giant SOT and magnetization switching induced by the in-plane current were recently revealed in various TI/magnet heterostructures [32, 33]. Figure 2 shows four stable states where the applied d.c. current conducts along the longitudinal direction ($\pm y$ axis) with the external magnetic field also applied along the $\pm y$ axis. It was found that, in the presence of a constant external magnetic field in the y direction, the z-component magnetization M_z can be switched by changing the d.c. current direction. When the applied d.c. current is fixed, M_z can also be switched by changing the in-plane external magnetic field. The resulted spin-Hall angle at low temperature was shown to be nearly three orders of magnitude larger than that in heavy metal cases. In short, both STT and SOT hereby demonstrate potential applications for low-power magnetization switching. Combined with recent studies about topological spintronics, fast domain wall, skyrmion motion, and tunable nano-oscillators based on TIs could bring about next-generation spintronic devices [34, 35].

2.2 Spin-charge conversion in TIs

Creation, detection, and manipulation of electrons' spins are key prerequisites for spintronics. From this point of view, TIs exhibit advantages by showing ultrahigh efficiencies in (1), converting electrical charge current into spin accumulation due to the helical locking of the topological surface states, or (2), vice versa, the spin to charge injection on the topological surface states using spin pumping, spin-polarized tunneling [36], etc. In case (1)

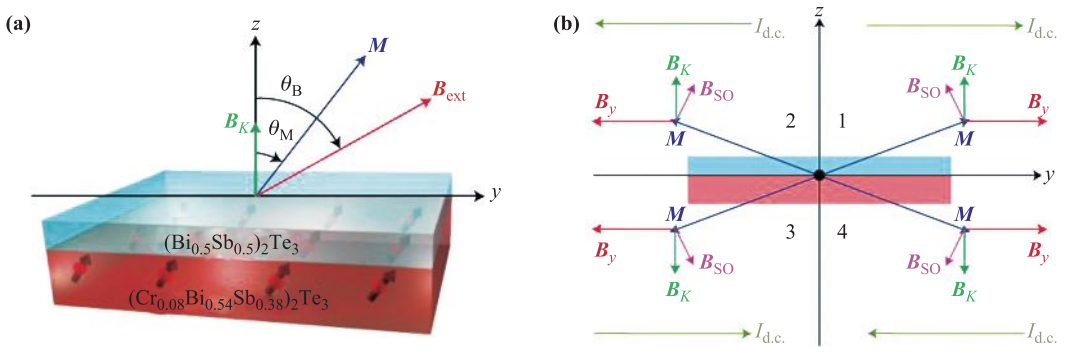

Fig. 2 **(a)** Schematic of the heterostructure. $\boldsymbol{B}_{\rm ext}$ (red arrow) represents the external magnetic field and $\boldsymbol{M}$ (blue arrow) denotes the magnetization of the bottom magnetic TI layer. $\boldsymbol{B}_K$ (green arrow) is the out-of-plane anisotropy field. **(b)** Schematic of the four stable magnetization states (panels 1–4) when passing a large d.c. current, and applying an in-plane external magnetic field, $\boldsymbol{B}_y$, in the $\pm y$ directions. The effective spin–orbit field $\boldsymbol{B}_{\rm SO}$ induced by the d.c. current and the anisotropy field $\boldsymbol{B}_K$ are both considered. Reproduced from Ref. [32].

of a TI/ferromagnet thin-film heterostructure, as shown in Fig. 3, when the ferromagnet resonates, the magnetization precession generates a non-equilibrium spin accumulation near the interface with the polarization axis parallel to the precession axis of the TI [37]. Such a spin pumping process can exert a torque on the precessing magnetization of the ferromagnet, which leads to an enhancement in the Gilbert damping constant. The induced non-equilibrium spin on the TI surfaces can further induce a charge current along the transverse direction, $\boldsymbol{z}\times\boldsymbol{\sigma}$, where $\boldsymbol{\sigma}$ is the spin polarization direction and $\boldsymbol{z}$ is the perpendicular unit vector. Note that the spin polarization on the topological surface states $\langle\boldsymbol{\sigma}_y\rangle$ is induced by the spin pumping driven by the ferromagnetic resonance. Owing to the helical locking in the topological surface states, the spin polarization gives rise to a shift of the Fermi circle of the Dirac fermions toward the x-direction. This induces a transverse electric field $E_x = -[4\pi\hbar/(ek_F\tau)](\langle\sigma_y\rangle/A)$, where k_F, τ, and A are the Fermi momentum, the scattering time of the Dirac fermions, and the unit area for the spin polarization, respectively. The effect described above is the so-called spin-charge conversion effect induced by spin pumping in the TI system, which is different from the case (2) that the spin current is converted into a charge current. The spin-charge conversion effect was further verified by the observation of the inverse Edelstein effect in a TI/ferromagnet (α-Sn/Fe) heterostructure, in which a vertical spin current injected into the TI surface can induce a charge current perpendicular to its own direction at the interface [30]. As shown in Fig. 4, this inverse Edelstein effect is produced by the counterclockwise helical spin configuration of the surface Dirac cone.

The spin to charge conservation is also supported by recent observations of the unidirectional spin-Hall effect and Rashba–Edelstein magnetoresistance in various TI/ferromagnet heterostructures [38, 39]. For example, in a magnetic TI/TI heterostructure as shown in Fig. 5, the current-dependent magnetoresistance was found to be quadratic in the applied voltage and linear in the magnetization. A possible mechanism of this effect is the coupling between the spin–orbit interaction and spin-dependent scattering with the current-induced spin accumulation to the electrical conductivity, which may relate to the interface and bulk spin-dependent electron scattering and

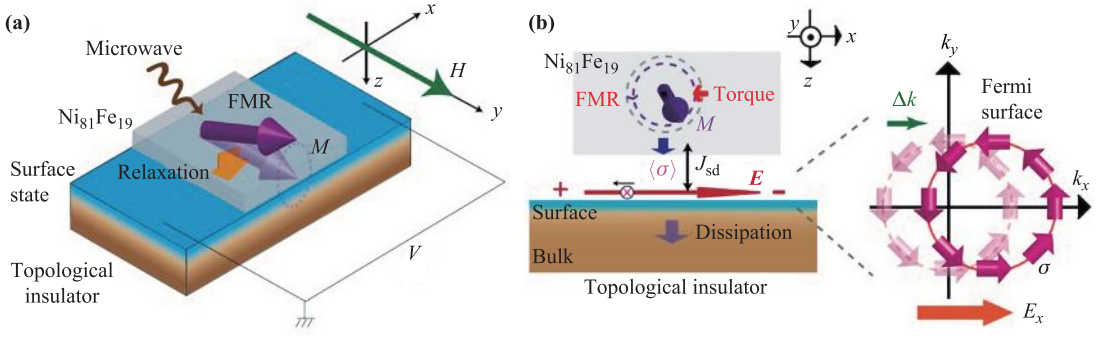

Fig. 3 **(a)** A schematic illustration of the experiment of the spin-electricity conversion effects. **(b)** Theoretical mechanism. The spin polarization on the surface state is induced by the spin pumping driven in the ferromagnet. Owing to the spin-momentum locking in the topological surface state, the spin polarization per unit area gives rise to a shift of the Fermi circle of the helical Dirac fermions, which induces the Hall signal. Reproduced from Ref. [37].

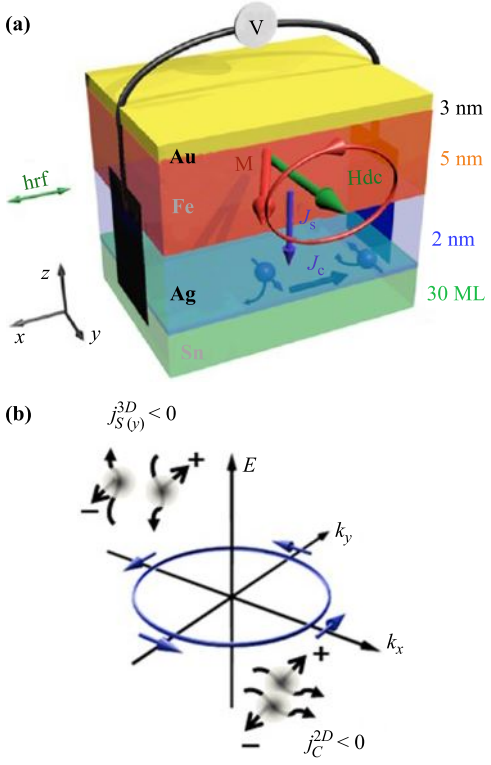

Fig. 4 **(a)** Experimental setup for spin pumping into α-Sn by ferromagnetic resonance of a Fe layer. **(b)** Fermi contours with helical spin configurations of TI surface or interface states. Reproduced from Ref. [30].

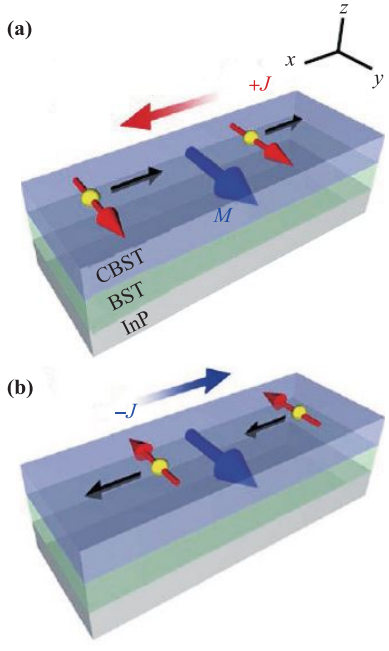

Fig. 5 Schematic illustration of the concept for unidirectional magnetoresistance in TI heterostructures under positive current **(a)** and negative d.c. current **(b)**. Here, magnetic field, magnetization, and dc current are along the in-plane direction, where dc current is applied perpendicular to the magnetization direction. Reproduced from Ref. [38].

electron–magnon scattering. When the spin accumulation is generated by the helical locking of the surface Dirac fermions and the strong SOC in the TI, these spins at the interface exhibit different conductances depending on the relative directions between the spin and the magnetization of the ferromagnet (magnetic TI, in this case). In this way, low and high conductance states can be accordingly identified, which enables a two-terminal spintronic device based on the unidirectional spin-Hall effect.

2.3 Topological antiferromagnetic spintronics

In addition to the TI/ferromagnet heterostructures, recent developments in heterostructures consisting of an antiferromagnetic (AFM) layer and a TI layer also demonstrated rich physics at the interface. At this interface, the surface Dirac fermions in the TI interact with the terminating magnetic atoms on the AFM surface, giving rise to emergent effects, although the AFM layer does not have macroscopic magnetization. One of these important effects is the induced interfacial ferromagnetic order. Such a ferromagnetic order can also break the time-reversal symmetry of the TI surface, similar to that of the TI/ferromagnet interface, which induces a finite Berry curvature and thus an anomalous Hall effect. Furthermore, since the AFM layer does not produce any stray field and is inert to a large external magnetic field, this induced ferromagnetic order should be robust against the external magnetic perturbations and moderate current, minimizing the crosstalk between devices and improving the device scalability. Besides, as this ferromagnetic order is originated from the AFM layer, its ordering temperature, i.e., the Curie temperature, largely depends on the Néel temperature of the AFM layer. Thus, the ferromagnetic order can survive at a much higher temperature than that in typical magnetically doped TIs. A typical example is that the antiferromagnet with a type-A Néel order, CrSb, enables an effective manipulation to the interfacial magnetic order and quantum states in the TI/antiferromagnet heterostructures [40]. As shown in Fig. 6, emergent interfacial magnetic interactions, including interfacial exchange coupling and antiferromagnetic exchange coupling, can be tailored through engineering artificial structures such as bilayers, trilayers, and superlattices. This antiferromagnet acts as efficient interfacial- and interlayer-exchange coupling mediators for the massive Dirac fermions of the TI, which additionally gives rise to an enhancement of the magnetic ordering temperature by a factor of three to that of a magnetically doped TI thin film.

More interestingly, due to the vanishingly small stray field in the AFM CrSb, the magnetization reversals of the top and bottom TI surfaces can be individually controlled, giving rise to additional intermediate spin configurations and hence topological transitions [41]. Strikingly, when the AFM layer was epitaxially grown on a TI thin film, a proximity-induced AHE was observed. This indicates that

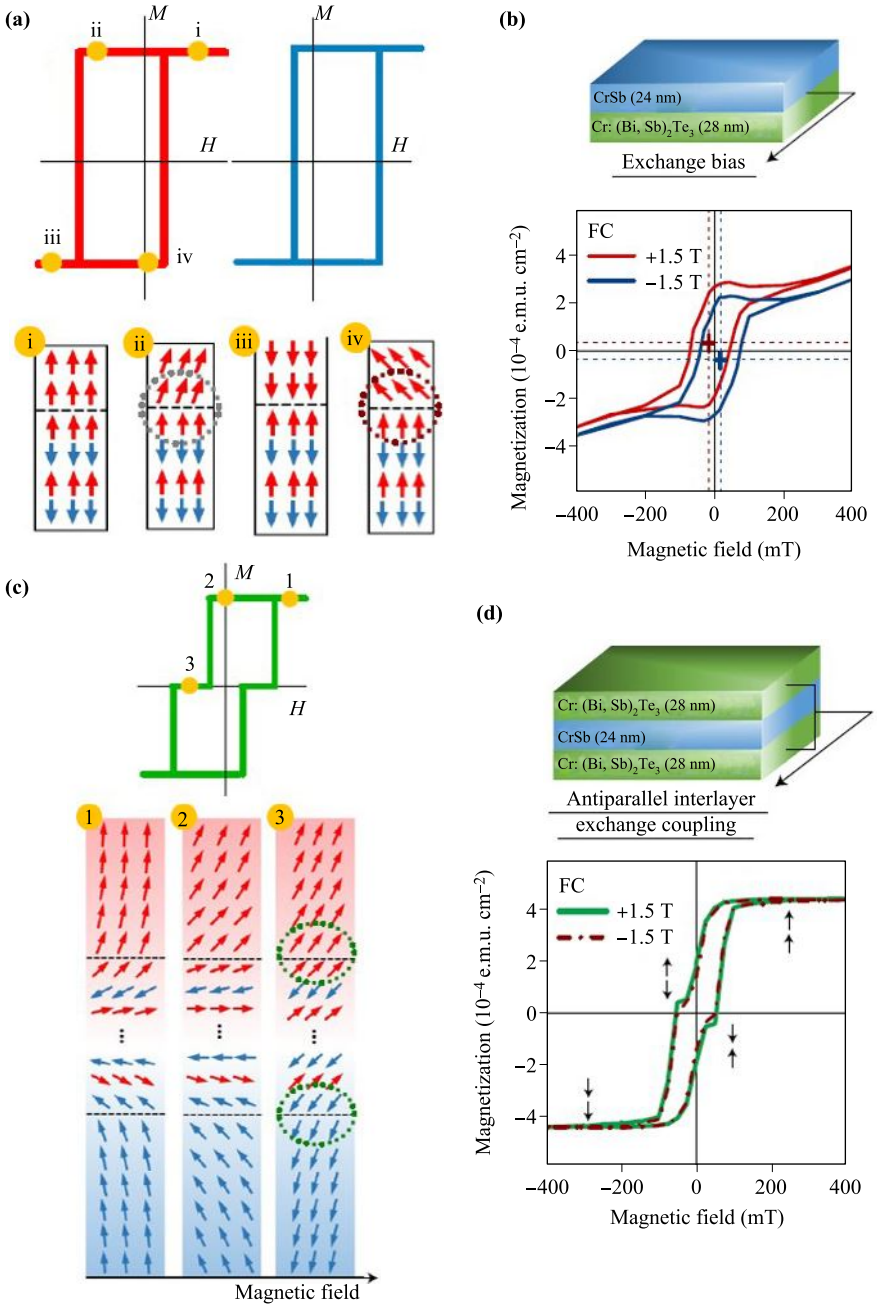

Fig. 6 **(a)** The schematic orientations of the atomic moments in the exchange-biased TI/antiferromagnet bilayer, illustrating strong magnetic interactions between the TI surface spins and the AFM spins. When the external field reverses the magnetization of the TI, the AFM spins do not follow the field but try to keep the ferromagnetic spins in their original orientations. Consequently the external field to reverse an exchange-biased TI is larger than for a single TI layer. **(b)** Exchange bias observed in a TI/antiferromagnet bilayer is demonstrated by the lateral shift (marked by dashed lines and crosses) of the M–H loops (red and blue) under different perpendicular field-coolings. Cooling in a positive field results in a negative shift (red loop, −10.8 mT) and vice versa (blue loop, +11.0 mT). **(c)** The relative orientations of the atomic moments of the effective long-range exchange coupling in a TI/antiferromagnet/TI trilayer, which is generated from a LLG quantitative simulation and calculation. **(d)** A novel antiparallel effective long-range exchange coupling is observed in the trilayer, which supports that this texture is mediated by the interactions between the TI surface spins and AFM spins. Reproduced from Ref. [40].

the polarized TI surface spins contribute extra magnetic moments to the saturated magnetization. Furthermore, both the Hall and the magneto-resistance measurements exhibit hysteresis which gradually vanishes as the temperature increases to 90 K, much higher than a magnetic TI (~30 K). Surprisingly, when introducing one additional AFM layer to produce an AFM/TI/AFM sandwich structure, another distinct magnetic feature is revealed. That

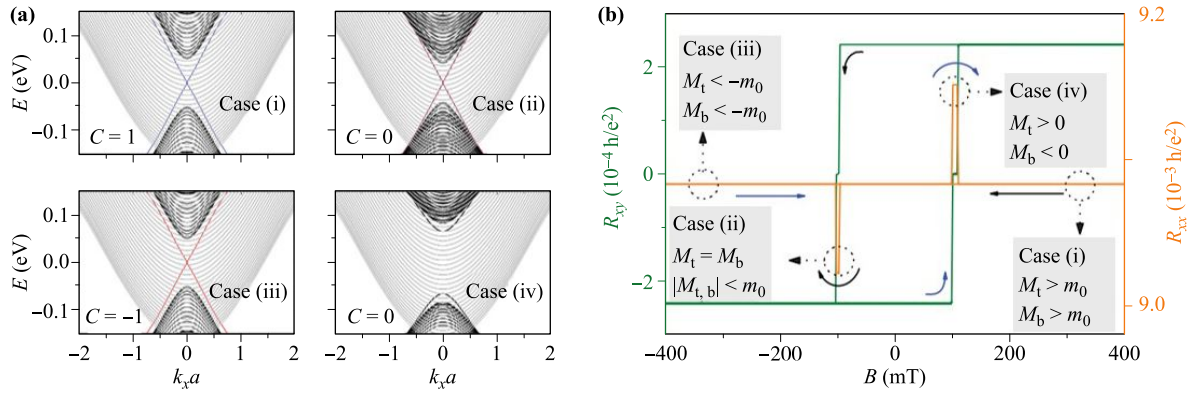

Fig. 7 **(a)** The black solid lines show the energy spectrum of a TI thin film with different top-bottom spin configurations. The grey lines indicate the parabolic bands from the AFM layers. The grey lines show the parabolic bands given by the AFM layers, while the black solid lines demonstrate the TI surface bands. **(b)** The evolution of the longitudinal resistance and the Hall resistance during the unsynchronized magnetic switching. The solid black arrows and the blue arrows denote the positive-to-negative and negative-to-positive field scan, respectively. Reproduced from Ref. [41].

is, magnetoresistance curves show antisymmetric spikes during the magnetization reversal process, as shown in Fig. 7, and these spikes occur when the corresponding anomalous Hall resistance changes sign. Meanwhile, both the spike-to-spike distance in the MR curve and the coercivity of the Hall loop have a temperature dependence which closely matches that of the AFM/TI case with a phase change temperature of around 90 K, underscoring the importance of the interfacial magnetic proximity effect induced by two AFM layers. This antisymmetric magnetoresistance contrasts sharply with the symmetric one observed in most ferromagnetic systems. A new topological transition was proposed to explain such observations. New topological orders, such as the axion insulating phase and a new phase with counter-propagating edge modes due to the unsynchronized magnetic switchings, are allowed to be manipulated using the antiferromagnets (Fig. 7).

Constructing TI-based heterostructures using antiferromagnets with different anisotropies can further modulate the spin-texture topological transition according to the polarization of anchoring spins in the AFM layer. Details will be discussed in the next section. Interfacing the TI with antiferromagnets unveils new avenues towards topological antiferromagnetic spintronics.

3 Magnetic skyrmions in TIs

Scalar spin chirality arisen from a modulation of spin structure through Dzyaloshinsky–Moriya interaction is the origin of the recently discovered geometric Hall effect. Such an effect is a probe to the non-trivial topological spin texture in real space, such as magnetic skyrmions. The topological surface states in TIs can also mediate Dzyaloshinsky–Moriya interaction among different magnetic moments due to the helical spin-momentum locking. As a result, these chiral magnetic structures can also appear on the TI surfaces. An possible observation of such magnetic skyrmions in TIs was discovered in a magnetic TI/nonmagnetic TI heterostructure [42]. Transport measurements in this heterostructure unveil the coexistence of the geometric Hall effect, which relates to the real-space Berry curvature from Néel-type skyrmions, and the anomalous Hall effect due to the momentum-space counterpart from the nontrivial Berry curvature in the TI layer (Fig. 8). Later, transport studies of Mn-doped Bi_2Te_3 thin films again show the appearance of similar geometric Hall

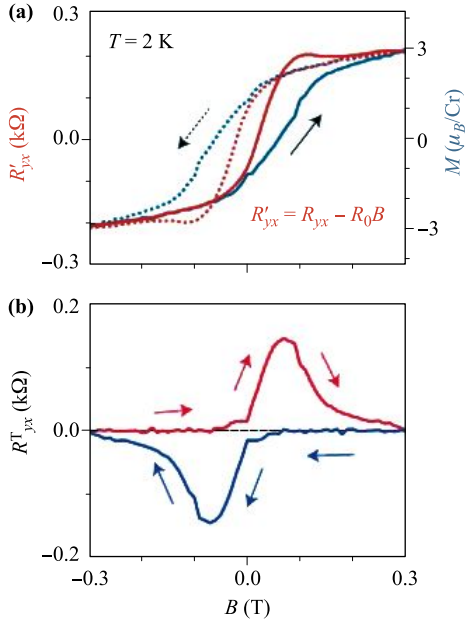

Fig. 8 **(a)** Magnetic-field dependence of Hall resistance after subtracting the normal Hall resistance (brown line) compared with the magnetization (blue line) for a TI/magnetic TI heterostructure. **(b)** Topological Hall component. Red (blue) curve represents the process for increasing (decreasing) magnetic field. Reproduced from Ref. [42].

effect in the magnetic TI thin film [43]. Surprisingly, in this Mn-doped Bi_2Te_3, the geometric Hall effect only exists in a thin film with certain thickness, and disappears otherwise. Such an observation reveals the important role played by the coupling between the top and bottom surface states of the TI thin film at a dimensional crossover regime, which can stabilize the magnetic skyrmion structure and is responsible for the resulting geometric Hall effect. The geometric Hall effect was also reported at the interface of a TI/antiferromagnet [$(Bi, Sb)_2Te_3$/MnTe] thin-film heterostructure [44]. More importantly, an interesting exchange bias effect is observed in the geometric Hall component, underscoring the coupling between the pinned Dirac electrons in the TI surface and the AFM spins. This exchange bias is reflected not only by a typical lateral shift of the entire Hall signal but also the magnitude switch of the geometric Hall component as shown in Fig. 9, which is given by the nucleation of skyrmions in an anchored AFM spin lattice. This TI/antiferromagnet heterostructure system is a novel platform to understand the physics of magnetic skyrmions in TIs and provides a new method to manipulate the nucleation of skyrmions using the AFM order.

4 Topological superconductor and Majorana fermion

Topological superconductor is a novel quantum state of matter that is adiabatically distinct from the superconducting state formed by Bose–Einstein condensate of Cooper pairs [2, 45, 46]. Among the topological superconductor family, two-dimensional topologically superconductors [47] were theoretically studied by Read and Green [48], while a one-dimensional model was proposed by Kitaev [49]. Both models consider spinless and time-reversal symmetry breaking for the superconducting states with p-wave pairing, which can host a non-Abelian Majorana zero mode at the edge in the one-dimensional case and in the vortex core in the two-dimensional case. Here, Majorana zero mode refers to the bound state of a Majorana fermion trapped in the vortex core of the superconductor. In particle physics, Majorana fermion is an elemental particle that is its own anti-particle. In condensed matter physics, this nature still holds; furthermore, Majorana fermion can be described using a superposition of electron and hole excitations. When their creation operators are identical to their annihilation operators respectively, such a quasi-particle or excitation is identified as a Majorana fermion. The emergence of such an excitation is the most prominent characteristic of a topological superconductor, which is useful as a topological qubit for application in topological quantum computation [2, 45, 50].

During the last couple of years, many theoretical proposals suggested that Majorana fermions can be created using artificial structure in solid-state devices. Experimentally, there are quite a few systems that were reported to host Majorana fermions, but the scope of this review is limited to the TI system. Relevant observations which can be interpreted as signatures of Majorana fermions are following.

4.1 Zero-bias anomaly

In 2008, Fu and Kane predicted a one-dimensional Majorana mode at the interface between a conventional s-wave superconductor and a TI when superconductivity is induced on the topological states by superconducting

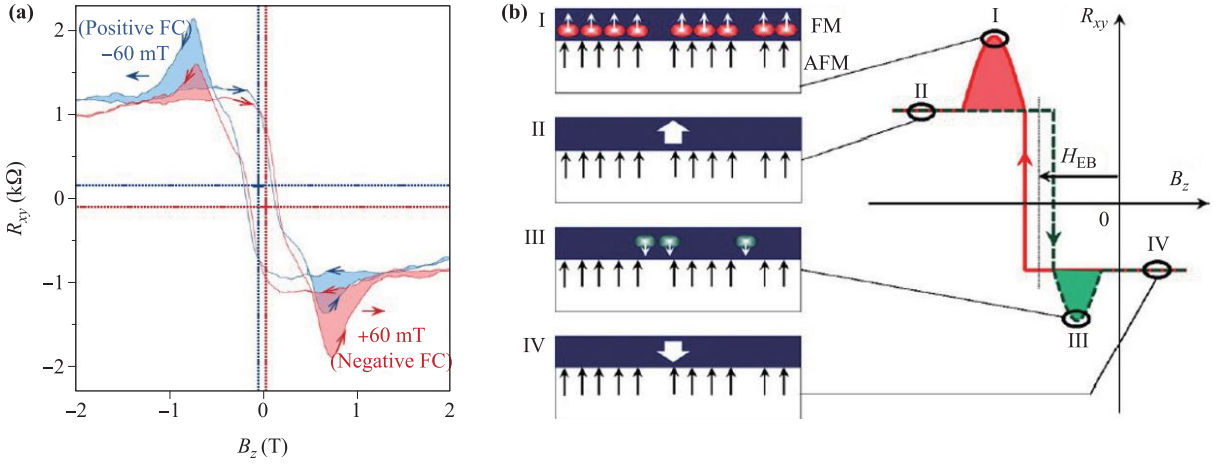

Fig. 9 **(a)** Hall resistance obtained in an applied perpendicular field from a TI/MnTe heterostructure. The dashed lines indicate the lateral shifts of the Hall signal. The colored areas show the magnitude change of the peak and dip regions referring to the geometric Hall effect. This magnitude change along with the lateral shift is the signature of the exchange-biased geometric Hall effect. **(b)** A schematic demonstration of the exchange-biased topological charges. The anchoring spins in the AFM layer assist the nucleation of positive topological charges (red circles) while prohibit the negative ones (green circles). Reproduced from Ref. [44].

proximity effect [24]. Majorana fermion is trapped within the vortex core of such a topological superconductor. Indeed, it is extremely difficult to experimentally distinguish them from other trivial states with a similar energy scale. To solve such a problem, techniques that can resolve the space and spin such as scanning tunneling microscopy have been adopted to probe the Majorana zero mode. For example, in a heterostructure consisting of a TI (Bi_2Se_3 or Bi_2Te_3) on top of an *s*-wave superconductor ($NbSe_2$), the spatial profile of the energy mode and the quasiparticle states within a vortex of the TI film were investigated using scanning tunneling microscopy with the results shown in Fig. 10. Superconducting pairing gap was found on the TI surface, which laid out an important material platform to explore the Majorana fermion [51]. By systematically investigating the spatial profile of the Majorana mode and the bound quasiparticle states within a vortex in the TI, it was found that, while a zero bias peak in local conductance splits right off the vortex center in conventional superconductors, it splits off at a finite distance away from the vortex center in the TI/superconductor heterostructure. This observation was attributed to a signature of the Majorana zero mode. Later, spin-selected

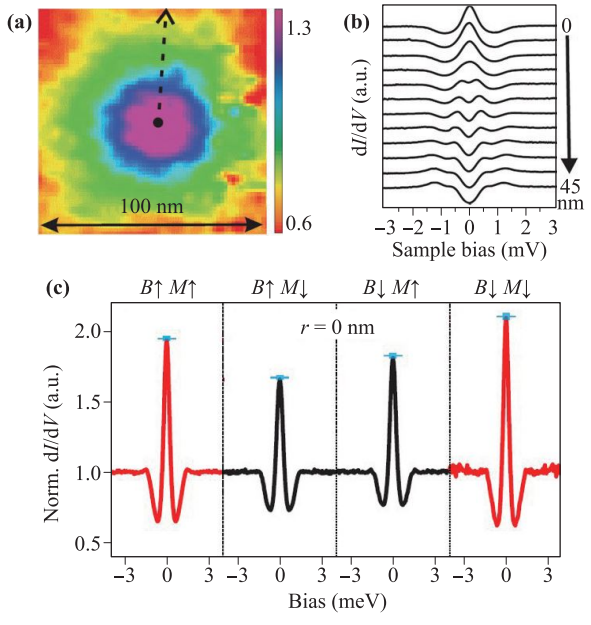

Fig. 10 **(a)** A vortex mapped by zero-bias dI/dV on 5 nm of $Bi_2Te_3/NbSe_2$ at 0.1 T and 0.4 K. **(b)** A series of dI/dV curves measured along the black dashed line in (a), showing the peak of bound states splits into two at positions away from the vortex center. **(c)** dI/dV at the vortex center measured with a fully spin polarized tip. Red curves are for tip polarization M parallel to magnetic field B, and black curves are for M antiparallel to B. In the measurements, $B = 0.1$ T and temperature $T = 30$ mK. The blue lateral lines give the average values of the intensities in multimeasurements, the vertical bars are the standard error bars. The intensity of the conductance with M parallel to B is about 14% higher than that with M antiparallel to B. Reproduced from Refs. [51, 52].

Andreev reflection experiments were carried out to further explore the energy states in the vortex [52]. Surprisingly, the magnitude of the zero-bias peak is substantially higher when the tip polarization and the external magnetic field are parallel. This spin-dependent tunneling effect provides another evidence of Majorana zero mode in this material system. Similar zero-bias anomaly was also reported in various TI/superconductor heterostructures, such as Bi_2Se_3/Sn [53] and Bi_2Se_3/NbN [54], revealed in quantum transport experiments. In these heterostructures, zero-bias conductance peaks in the conductance spectra were observed below the superconducting transition temperature of the superconducting electrodes, which indicates the important role played by the superconductivity. These observations may reveal that a proximity-effect-induced unconventional superconducting phase is formed at the interface. In a TI (Bi_2Se_3) thin film contacted by superconducting (In, Al, and W) electrodes, conductance anomalies were also observed and attributed to the interplay between the Cooper pairs of the electrodes and the spin-polarized current of the surface states in the TI [55]. Anomalous conductance spectra were investigated in some doped TIs such as Cu-doped Bi_2Se_3 [56] (see Fig. 11) and In-doped SnTe [57], which exhibit intrinsic superconductivity. Both materials systems indicate possible intrinsic topological superconductivity and odd-parity pairing favored by strong SOC. Induced superconductivity on the TI surfaces was also reported in TI/high-temperature superconductor heterostructures [58, 59].

4.2 Unconventional Josephson effect

Based on Fu and Kane's prediction, in a Josephson junction consisting of two superconducting electrodes on the top of a TI, the boundaries of the two materials are expected to host two one-dimensional Majorana modes, giving rise to a one-dimensional wire of Majorana fermions running along the edges of the device. One striking characteristic of such a device is the unconventional Fraunhofer-like magnetic diffraction pattern, in which the first minimum in critical current density should occur when one flux quantum of $h/(2e)$ passes through the area

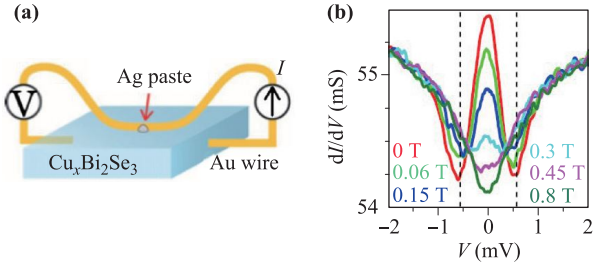

Fig. 11 **(a)** Sketch of the soft point contact and the measurement circuit in the point-contact experiment. **(b)** The spectra at 0.35 K measured in perpendicular magnetic fields of 0–0.8 T. The vertical dashed lines indicate the energy position of the dips. Reproduced from Ref. [56].

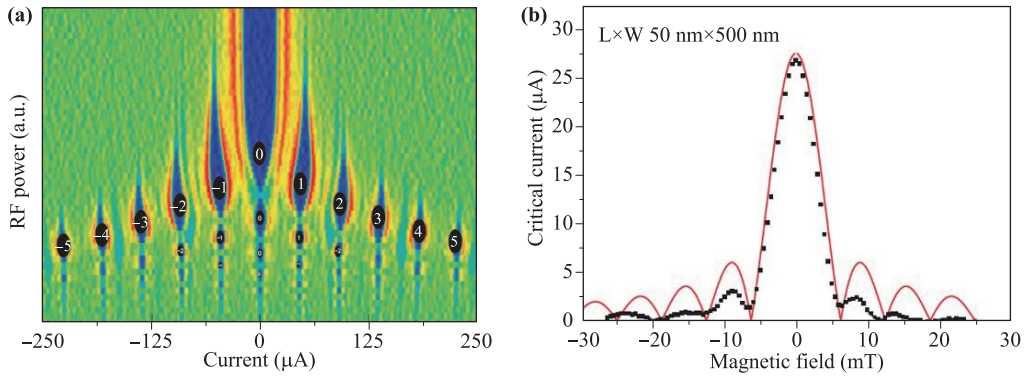

Fig. 12 **(a)** Differential resistance, $\mathrm{d}V/\mathrm{d}I$, plotted on a colour scale as a function of the bias current, I, and the microwave excitation power. The numbers correspond to the nth order Shapiro step. **(b)** Critical current dependence on the magnetic field, fitted with $I_C = I_0|\mathrm{sinc}(\pi\Phi/\Phi_0)|$, where I_0 is the critical current at zero field, Φ the flux and Φ_0 the flux quantum. Reproduced from Ref. [60].

of the device. Recent experiments using superconductor-TI-superconductor Josephson junctions supported such a prediction. In a lateral Nb–Bi_2Te_3–Nb Josephson junction, it was shown that the observations of clear Shapiro steps under microwave irradiation and a Fraunhofer-type dependence of the critical current on magnetic field together implied the existence of the Majorana modes (Fig. 12) [60]. Therefore, the topological surface states indeed carry the ballistic Josephson current. The unconventional Fraunhofer-like magnetic diffraction pattern was also observed in a Pb–Bi_2Te_3–Pb Josephson junction [61]. Furthermore, as shown in Fig. 13, it was reported that, in a Nb–Bi_2Se_3–Nb Josephson junction, two striking distinctions from the common Josephson junction behavior were observed, i.e., the characteristic energy was found to inversely scale with the width of the junction, and a low characteristic magnetic field can suppress supercurrent [62]. These features were explained using a twofold phenomenological extension to the model with both extensions arising from confinement along the length of the Majorana wire. Besides the three-dimensional TI family $(Bi, Sb)_2(Te, Se)_3$, the TI system in two-dimension, HgTe quantum well, acts as another versatile platform for investigating the topological superconductivity and Majorana fermions. In 2012, superconductivity was induced in a (Nb–HgTe–Nb) Josephson junction, in which unconventional periodic oscillations of the differential resistance as a function of an applied magnetic field were observed, showing a Fraunhofer-like pattern [63]. This material system was regarded as a precursor of the Josephson effect occurred in the topological edge states of the HgTe system. Later, further investigations in this system showed that supercurrents were indeed confined to the one-dimensional sample edges when the TI bulk density was depleted, as shown in Fig. 14. In 2016, Bocquillon *et al.* [64] observed a supercurrent with a 4π periodicity in the superconducting phase difference using the a.c. Josephson effect in this material system, as indicated by a doubling of multiple Shapiro steps. Such a signature also implies that the 4π-periodic supercurrent originates in states located on the edges of the junction.

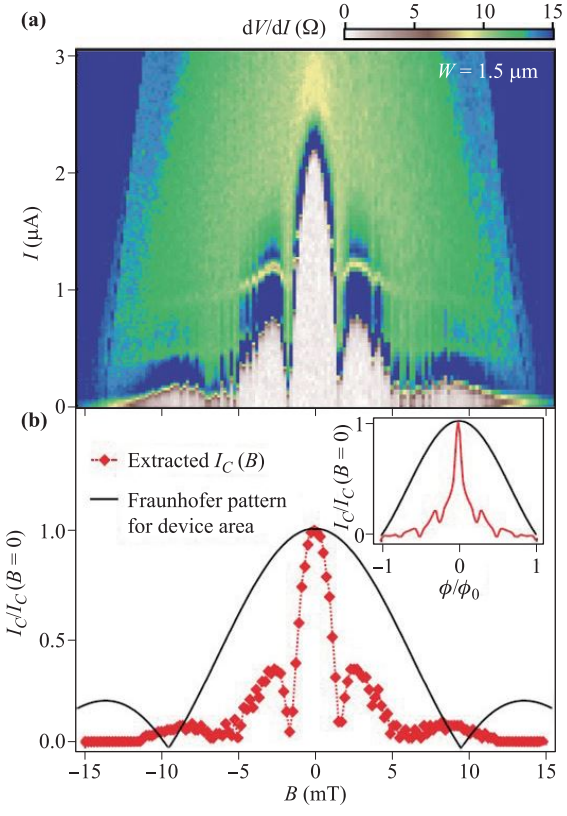

Fig. 13 **(a)** Differential resistance $\mathrm{d}V/\mathrm{d}I$ as a function of B and I showing an anomalous magnetic diffraction pattern. **(b)** $I_C(B)$ (dashed line with circles) extracted from $\mathrm{d}V/\mathrm{d}I$ in (a) is compared to the expected Fraunhofer pattern for the junction (solid line) where a reduction of the scale of the pattern and the nonuniform spacing are evident. Inset: A comparison of the simulated Frauhofer pattern for a sinusoidal and an empirically determined, peaked current phase relation. Reproduced from Ref. [62].

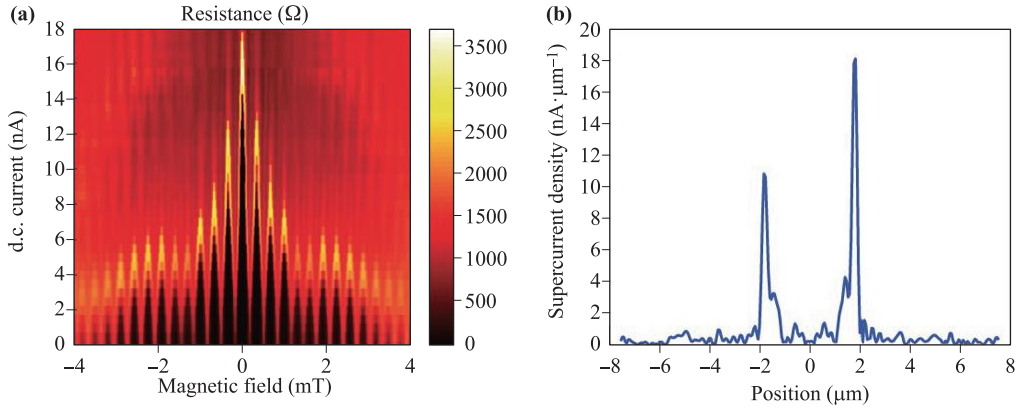

Fig. 14 **(a)** The differential resistance shows a sinusoidal interference pattern. **(b)** Using the interference envelope, the supercurrent density is clearly dominated by the contribution from the edges. In this regime almost no supercurrent passes through the bulk. Reproduced from Ref. [80].

4.3 Momentum-space imaging

The helical spin-momentum locking on the surface of TIs is in contrast to the Fermi level electronic states of an ordinary superconductor. If superconductivity is induced on the TI surface, helical-Cooper pairing should be defined as the superconducting Bose condensation of the spin-momentum-locked Dirac electron gas. To further identify this state, a spin- and momentum-resolved technique is needed. The first demonstration of the coexistence of topological property and superconductivity on the TI surface was discovered in a $Bi_2Se_3/NbSe_2$ heterostructure using both scanning tunneling microscopy and angle-resolved photoemission spectroscopy [65]. Similar heterostructure was further studied by Su *et al.* [66] by observing the momentum-resolved Bogoliubov quasi-particle spectrum of the TI thin film. The existence of Cooper pairing in this weakly interacting half Dirac gas was therefore identified, as shown in Fig. 15. The above studies revealed a two-dimensional topological superconductivity in the TI thin film, which was supported by the helical Cooper pairing in the spin-momentum-locked Dirac electron gas. The TI/*s*-wave superconductor system is distinct from that of an ordinary two-dimensional superconductor in terms of the spin degrees of freedom of electrons. More recently, it was found that the superconducting paring gap on the TI surface can also be induced by a *d*-wave high-temperature superconductor [67]. This was achieved by growing a TI thin film (Bi_2Se_3) on a *d*-wave superconductor substrate ($Bi_2Sr_2CaCu_2O_8$), as shown in Fig. 16. It was shown that the induced high-temperature superconductivity on the surface states of the TI thin film gave rise to a superconducting pairing gap as large as 15 meV. Interestingly, distinct from the *d*-wave pairing of $Bi_2Sr_2CaCu_2O_8$, the proximity-induced gap on the topological surface states is almost isotropic in the entire momentum space and consistent with predominant *s*-wave pairing.

4.4 Chiral edge mode

The induced superconducting pairing gap on the TI surface mentioned above is helical since the artificial structures were constructed using intrinsic TIs. Indeed, if the gapless topological surface states are open by exchange coupling due to magnetic impurities/dopants or magnetic proximity effect, time-reversal symmetry in the TI will be

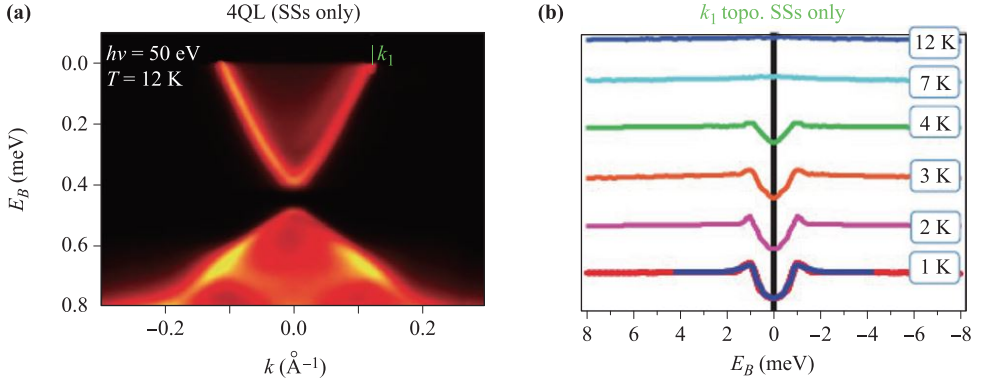

Fig. 15 **(a)** ARPES dispersion map of a 4nm Bi_2Se_3 film on $NbSe_2$. **(b)** Symmetrized ARPES spectra at fixed momentum k_1. Reproduced from Ref. [66].

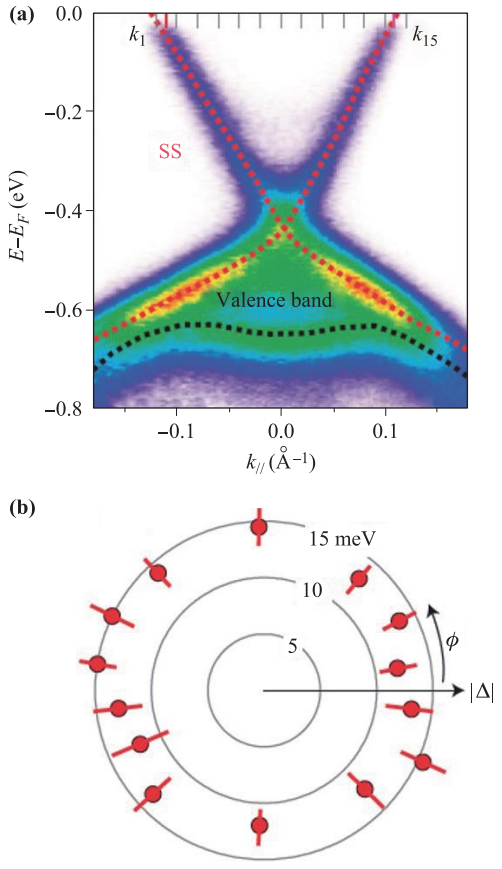

Fig. 16 **(a)** ARPES data of a $Bi_2Se_3/Bi_2Sr_2CaCu_2O_8$ heterostructure. Dotted lines are guides for the dispersions of surface states (SS) and valence band. **(b)** Azimuth (ϕ) dependence of the gap size (radial axis) along the Fermi surface. Reproduced from Ref. [67].

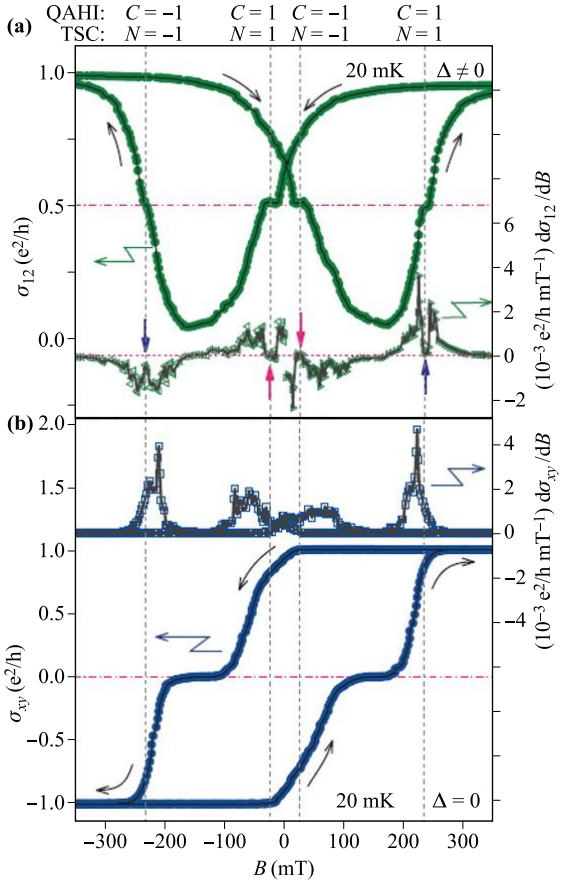

Fig. 17 **(a)** Longitudinal conductance σ_{12} as a function of external perpendicular magnetic field obtained at 20 mK. When superconductivity is induced on the top surface of the quantum anomalous Hall insulator (QHAI), σ_{12} shows additional half-integer plateaus (~ 0.5 e^2/h) between the transitions of the QAHI ($C = \pm 1$) and the normal insulator. (Lower plot) Derivative of σ_{12} with respect to the magnetic field. Topological transitions are marked by dashed lines and arrows. **(b)** Without superconducting proximity effect, the Hall conductance (σ_{xy}) of the QAHI device demonstrates the evolution between QAHI ($C = \pm 1$) and the normal insulator, illustrating the surface-hybridization–induced zero plateaus at the coercive fields during magnetization reversals. Reproduced from Ref. [68].

broken and a finite Berry curvature is introduced. This further creates an intrinsic anomalous Hall effect in the magnetic TI. Inside this exchange gap, nonzero Chern numbers of ± 1 arise, giving rise to a chiral edge mode which encircles the boundary of the TI and is topologically protected. In this case, if a superconducting pairing gap is induced to this system, a chiral topological superconductor with an odd-integer Chern number will be formed, which can also accommodate the peculiar Majorana fermions. As described above, most of the evidences for the Majorana bound states call for the observation of localizations of Majorana fermions within a topological defect/edge at zero energy. However, no report explicitly shows the Majorana fermion-associated quantum transport. Recently, a system consisting of a quantum anomalous Hall insulator fabricated with a magnetic topological insulator, Cr-doped $(Bi, Sb)_2Te_3$, whose top surface is partially covered by an s-wave superconducting film, Nb, is used to realize the chiral topological superconductor [68]. As shown in Fig. 17, the Majorana backscattering at the boundaries of this system gives rise to half-integer longitudinal conductance plateaus close to the predicted quantized value (0.5 e^2/h), which locate at the neighbor of the transitions between states with Chern number of ± 1 and 0 in the quantum anomalous Hall insulator. Such observations demonstrate the chiral Majorana fermion edge states in a chiral topological superconductor, which may lead to the development of topological quantum computation.

5 Outlook

Two main applications using TIs have been demonstrated in this review. The recent developments in the new realm of topological spintronics demonstrate the promising ap-

plications using TIs and other topological materials in spintronic devices, while the topological superconductor is prominent in theoretical physics since years ago, however, their experimental investigations remain in infancy. Such a contrast may be mainly due to the limited strategies and challenging difficulties in detection and manipulation of the Majorana fermion and topological superconductivity even using the state-of-the-art experimental techniques. Also, the area of spintronics is well-developed for decades and both theoretical and experimental aspects are much more mature than those in topological superconductivity and quantum computation. With the recent insights and developments in topological superconductor, it is foreseeable that Majorana fermions in condensed matter will soon become a well-grounded paradigm.

The helical locking and strong SOC in TI surfaces are the most important properties of TIs for application in topological spintronics. Next, it is insightful to make topological spintronic devices that are robust against external perturbations with a smaller device scale, a lower manipulation current density, and higher energy efficiency. Such an idea could be implemented in the emergent area of topological antiferromagnetic spintronics. The antiferromagnetic spintronics using both topological trivial and non-trivial matters coupled with antiferromagnets is among the most attractive topics in spintronics. The most important features of antiferromagnet are the robustness against perturbations induced by magnetic field, zero stray field, ultrafast dynamics, and capability of generating large magnetotransport effects. These features, however, also make the detection and manipulation of the AFM spins and AFM orders challenging when compared with the ferromagnet and ferrimagnet whose net magnetizations can be easily identified. These challenges may be addressed using the topological orders when considering the special spin texture in topological materials, such as the helical spin texture on TI surfaces. Furthermore, AFM order is also shown to allow a manipulation of the topological orders as well. These methods enrich the research in topological antiferromagnetic spintronics. While the magnetization switching at cryogenic temperature in TI-based heterostructures points out an important application for developing prototypic topological spintronic devices, logic/memory devices that enable switching at room-temperature using topological materials can make a further step towards industrial application [69]. This is supported by the observation of topological states at room temperature. Recently, the room-temperature magnetization switching with the help from TIs has been demonstrated using different TI heterostructures, including CoTb/Bi_2Se_3 [70], CoFeB/Bi_2Se_3 [71, 72] and MnGa/BiSb [73]. The fast developments in these two new directions consistently show the important roles played by TIs in spintronics.

It has been shown that both Majorana bound states and Majorana edge states allow topologically protected quantum gates and realization of the topological quantum computation [26, 74–78]. The Majorana bound states, which emerge in the bulk vortices of a p+ip topological superconductor [48] or at the endpoints of a one-dimensional p-wave superconducting chain [49, 79], are well known to obey non-Abelian braiding statistics. So far, the Majorana bound states in vortex cores of TI surfaces have been experimentally observed. However, the existence of these Majorana states still need further confirmation. Specifically, a stable quantized tunnel-conductance plateau, robust against variations in all gate voltages and magnetic field strength should be experimentally identified in tunneling spectroscopy experiments, etc. Moreover, new theoretical proposals based on the Majorana teleportation and interference using these Majorana bound states are urgently needed.

During the past decades, to realize topological quantum computation, tremendous efforts had been made in both theory and experiment using the Majorana bound states. However, due to the localized and dot-like characters of these states, all existing proposed architectures inevitably require nanoscale design, fabrication, and manipulation of the coupling among different Majorana bound states with high precision, which indeed challenge the further development of this area. In contrast, the Majorana edge states, which naturally accomplish the quantum computation by the propagation of the Majorana fermion wave packets at the edges. Such a propagation is physically equivalent to the braiding of Majorana bound states, which could be a promising approach for realizing the quantum gate for computation.

Acknowledgements We acknowledge the supports from the National Natural Science Foundation of China (Grant No. 11874070), the National Key R&D Program of China (Grant No. 2018YFA0305601), the Strategic Priority Research Program of Chinese Academy of Sciences (Grant No. XDB28000000), and National Thousand-Young-Talents Program in China (Grant No. 8206100161).

References

1. M. Z. Hasan and C. L. Kane, Colloquium: Topological insulators, *Rev. Mod. Phys.* 82(4), 3045 (2010)
2. X. L. Qi and S. C. Zhang, Topological insulators and superconductors, *Rev. Mod. Phys.* 83(4), 1057 (2011)
3. C. K. Chiu, J. C. Y. Teo, A. P. Schnyder, and S. Ryu, Classification of topological quantum matter with symmetries, *Rev. Mod. Phys.* 88(3), 035005 (2016)
4. P. Roushan, J. Seo, C. V. Parker, Y. S. Hor, D. Hsieh, D. Qian, A. Richardella, M. Z. Hasan, R. J. Cava, and A. Yazdani, Topological surface states protected from backscattering by chiral spin texture, *Nature* 460(7259), 1106 (2009)
5. T. Zhang, P. Cheng, X. Chen, J. F. Jia, X. Ma, K. He, L. Wang, H. Zhang, X. Dai, Z. Fang, X. Xie, and Q. K.

Xue, Experimental demonstration of topological surface states protected by time-reversal symmetry, *Phys. Rev. Lett.* 103(26), 266803 (2009)

6. K. Klitzing, G. Dorda, and M. Pepper, New method for high-accuracy determination of the fine-structure constant based on quantized Hall resistance, *Phys. Rev. Lett.* 45(6), 494 (1980)
7. D. J. Thouless, M. Kohmoto, M. P. Nightingale, and M. den Nijs, Quantized Hall conductance in a two-dimensional periodic potential, *Phys. Rev. Lett.* 49(6), 405 (1982)
8. J. E. Moore, The birth of topological insulators, *Nature* 464(7286), 194 (2010)
9. B. A. Bernevig, T. L. Hughes, and S. C. Zhang, Quantum spin Hall effect and topological phase transition in HgTe quantum wells, *Science* 314(5806), 1757 (2006)
10. M. Konig, S. Wiedmann, C. Brune, A. Roth, H. Buhmann, L. W. Molenkamp, X. L. Qi, and S. C. Zhang, Quantum spin hall insulator state in HgTe quantum wells, *Science* 318(5851), 766 (2007)
11. D. Hsieh, D. Qian, L. Wray, Y. Xia, Y. S. Hor, R. J. Cava, and M. Z. Hasan, A topological Dirac insulator in a quantum spin Hall phase, *Nature* 452(7190), 970 (2008)
12. Y. Xia, D. Qian, D. Hsieh, L. Wray, A. Pal, H. Lin, A. Bansil, D. Grauer, Y. S. Hor, R. J. Cava, and M. Z. Hasan, Observation of a large-gap topological-insulator class with a single Dirac cone on the surface, *Nat. Phys.* 5(6), 398 (2009)
13. C. L. Kane and E. J. Mele, Z2 topological order and the quantum spin Hall effect, *Phys. Rev. Lett.* 95(14), 146802 (2005)
14. L. Fu, C. L. Kane, and E. J. Mele, Topological insulators in three dimensions, *Phys. Rev. Lett.* 98(10), 106803 (2007)
15. H. Zhang, C. X. Liu, X. L. Qi, X. Dai, Z. Fang, and S. C. Zhang, Topological insulators in Bi_2Se_3, Bi_2Te_3 and Sb_2Te_3 with a single Dirac cone on the surface, *Nat. Phys.* 5(6), 438 (2009)
16. N. P. Armitage, E. J. Mele, and A. Vishwanath, Weyl and Dirac semimetals in three-dimensional solids, *Rev. Mod. Phys.* 90(1), 015001 (2018)
17. D. Hsieh, Y. Xia, L. Wray, D. Qian, A. Pal, J. H. Dil, J. Osterwalder, F. Meier, G. Bihlmayer, C. L. Kane, Y. S. Hor, R. J. Cava, and M. Z. Hasan, Observation of unconventional quantum spin textures in topological insulators, *Science* 323(5916), 919 (2009)
18. Y. L. Chen, J. G. Analytis, J. H. Chu, Z. K. Liu, S. K. Mo, X. L. Qi, H. J. Zhang, D. H. Lu, X. Dai, Z. Fang, S. C. Zhang, I. R. Fisher, Z. Hussain, and Z. X. Shen, Experimental realization of a three-dimensional topological insulator, Bi_2Te_3, *Science* 325(5937), 178 (2009)
19. D. Hsieh, Y. Xia, D. Qian, L. Wray, J. H. Dil, F. Meier, J. Osterwalder, L. Patthey, J. G. Checkelsky, N. P. Ong, A. V. Fedorov, H. Lin, A. Bansil, D. Grauer, Y. S. Hor, R. J. Cava, and M. Z. Hasan, A tunable topological insulator in the spin helical Dirac transport regime, *Nature* 460(7259), 1101 (2009)
20. A. R. Mellnik, J. S. Lee, A. Richardella, J. L. Grab, P. J. Mintun, M. H. Fischer, A. Vaezi, A. Manchon, E. A. Kim, N. Samarth, and D. C. Ralph, Spin-transfer torque generated by a topological insulator, *Nature* 511(7510), 449 (2014)
21. Y. Fan and K. L. Wang, Spintronics based on topological insulators, *Spin* 06(02), 1640001 (2016)
22. R. Yu, W. Zhang, H. J. Zhang, S. C. Zhang, X. Dai, and Z. Fang, Quantized anomalous Hall effect in magnetic topological insulators, *Science* 329(5987), 61 (2010)
23. J. Wu, J. Liu, and X. J. Liu, Topological spin texture in a quantum anomalous Hall insulator, *Phys. Rev. Lett.* 113(13), 136403 (2014)
24. L. Fu and C. L. Kane, Superconducting proximity effect and majorana fermions at the surface of a topological insulator, *Phys. Rev. Lett.* 100(9), 096407 (2008)
25. J. Wang and S. C. Zhang, Topological states of condensed matter, *Nat. Mater.* 16(11), 1062 (2017)
26. B. Lian, X. Q. Sun, A. Vaezi, X. L. Qi, and S. C. Zhang, Topological quantum computation based on chiral Majorana fermions, *Proc. Natl. Acad. Sci. USA* 115(43), 10938 (2018)
27. P. Deorani, J. Son, K. Banerjee, N. Koirala, M. Brahlek, S. Oh, and H. Yang, Observation of inverse spin Hall effect in bismuth selenide, *Phys. Rev. B* 90(9), 094403 (2014)
28. H. C. Han, Y. S. Chen, M. D. Davydova, P. N. Petrov, P. N. Skirdkov, J. G. Lin, J. C. Wu, J. C. A. Huang, K. A. Zvezdin, and A. K. Zvezdin, Spin pumping and probe in permalloy dots-topological insulator bilayers, *Appl. Phys. Lett.* 111(18), 182411 (2017)
29. A. A. Baker, A. I. Figueroa, L. J. Collins-McIntyre, G. van der Laan, and T. Hesjedal, Spin pumping in ferromagnet-topological insulator-ferromagnet heterostructures, *Sci. Rep.* 5(1), 7907 (2015)
30. J. C. Rojas-Sánchez, S. Oyarzun, Y. Fu, A. Marty, C. Vergnaud, S. Gambarelli, L. Vila, M. Jamet, Y. Ohtsubo, A. Taleb-Ibrahimi, P. Le Fevre, F. Bertran, N. Reyren, J. M. George, and A. Fert, Spin to charge conversion at room temperature by spin pumping into a new type of topological insulator: α-Sn films, *Phys. Rev. Lett.* 116(9), 096602 (2016)
31. C. N. Wu, Y. H. Lin, Y. T. Fanchiang, H. Y. Hung, H. Y. Lin, P. H. Lin, J. G. Lin, S. F. Lee, M. Hong, J. Kwo, Strongly enhanced spin current in topological insulator/ferromagnetic metal heterostructures by spin pumping, *J. Appl. Phys.* 117(17), 17D148(2015)
32. Y. Fan, P. Upadhyaya, X. Kou, M. Lang, S. Takei, Z. Wang, J. Tang, L. He, L. T. Chang, M. Montazeri, G. Yu, W. Jiang, T. Nie, R. N. Schwartz, Y. Tserkovnyak, and K. L. Wang, Magnetization switching through giant spin–orbit torque in a magnetically doped topological insulator heterostructure, *Nat. Mater.* 13(7), 699 (2014)
33. Y. Fan, X. Kou, P. Upadhyaya, Q. Shao, L. Pan, M. Lang, X. Che, J. Tang, M. Montazeri, K. Murata, L. T. Chang, M. Akyol, G. Yu, T. Nie, K. L. Wong, J. Liu, Y. Wang, Y. Tserkovnyak, and K. L. Wang, Electric-field control of spin–orbit torque in a magnetically doped topological insulator, *Nat. Nanotechnol.* 11(4), 352 (2016)

34. Z. Jiang, C. Z. Chang, M. R. Masir, C. Tang, Y. Xu, J. S. Moodera, A. H. MacDonald, and J. Shi, Enhanced spin Seebeck effect signal due to spin-momentum locked topological surface states, *Nat. Commun.* 7(1), 11458 (2016)
35. Y. Q. Huang, Y. X. Song, S. M. Wang, I. A. Buyanova, and W. M. Chen, Spin injection and helicity control of surface spin photocurrent in a three dimensional topological insulator, *Nat. Commun.* 8, 15401 (2017)
36. L. Liu, A. Richardella, I. Garate, Y. Zhu, N. Samarth, and C. T. Chen, Spin-polarized tunneling study of spin-momentum locking in topological insulators, *Phys. Rev. B* 91(23), 235437 (2015)
37. Y. Shiomi, K. Nomura, Y. Kajiwara, K. Eto, M. Novak, K. Segawa, Y. Ando, and E. Saitoh, Spin-electricity conversion induced by spin injection into topological insulators, *Phys. Rev. Lett.* 113(19), 196601 (2014)
38. Y. Lv, J. Kally, D. Zhang, J. S. Lee, M. Jamali, N. Samarth, and J. P. Wang, Unidirectional spin-Hall and Rashba–Edelstein magnetoresistance in topological insulator-ferromagnet layer heterostructures, *Nat. Commun.* 9(1), 111 (2018)
39. K. Yasuda, A. Tsukazaki, R. Yoshimi, K. S. Takahashi, M. Kawasaki, and Y. Tokura, Large unidirectional magnetoresistance in a magnetic topological insulator, *Phys. Rev. Lett.* 117(12), 127202 (2016)
40. Q. L. He, X. Kou, A. J. Grutter, G. Yin, L. Pan, X. Che, Y. Liu, T. Nie, B. Zhang, S. M. Disseler, B. J. Kirby, W. II Ratcliff, Q. Shao, K. Murata, X. Zhu, G. Yu, Y. Fan, M. Montazeri, X. Han, J. A. Borchers, and K. L. Wang, Tailoring exchange couplings in magnetic topological-insulator/antiferromagnet heterostructures, *Nat. Mater.* 16(1), 94 (2017)
41. Q. L. He, G. Yin, L. Yu, A. J. Grutter, L. Pan, C. Z. Chen, X. Che, G. Yu, B. Zhang, Q. Shao, A. L. Stern, B. Casas, J. Xia, X. Han, B. J. Kirby, R. K. Lake, K. T. Law, and K. L. Wang, Topological transitions induced by antiferromagnetism in a thin-film topological insulator, *Phys. Rev. Lett.* 121(9), 096802 (2018)
42. K. Yasuda, R. Wakatsuki, T. Morimoto, R. Yoshimi, A. Tsukazaki, K. S. Takahashi, M. Ezawa, M. Kawasaki, N. Nagaosa, and Y. Tokura, Geometric Hall effects in topological insulator heterostructures, *Nat. Phys.* 12(6), 555 (2016)
43. C. Liu, Y. Zang, W. Ruan, Y. Gong, K. He, X. Ma, Q. K. Xue, and Y. Wang, Dimensional crossover-induced topological Hall effect in a magnetic topological insulator, *Phys. Rev. Lett.* 119(17), 176809 (2017)
44. Q. L. He, G. Yin, A. J. Grutter, L. Pan, X. Che, G. Yu, D. A. Gilbert, S. M. Disseler, Y. Liu, P. Shafer, B. Zhang, Y. Wu, B. J. Kirby, E. Arenholz, R. K. Lake, X. Han, and K. L. Wang, Exchange-biasing topological charges by antiferromagnetism, *Nat. Commun.* 9(1), 2767 (2018)
45. F. Wilczek, Majorana returns, *Nat. Phys.* 5(9), 614 (2009)
46. J. Nilsson, A. R. Akhmerov, and C. W. Beenakker, Splitting of a Cooper pair by a pair of Majorana bound states, *Phys. Rev. Lett.* 101(12), 120403 (2008)
47. M. Sato and Y. Ando, Topological superconductors: A review, *Rep. Prog. Phys.* 80(7), 076501 (2017)
48. N. Read and D. Green, Paired states of fermions in two dimensions with breaking of parity and time-reversal symmetries and the fractional quantum Hall effect, *Phys. Rev. B* 61(15), 10267 (2000)
49. A. Y. Kitaev, Unpaired Majorana fermions in quantum wires, *Phys. Uspekhi* 44(10S), 131 (2001)
50. J. C. Teo and C. L. Kane, Majorana fermions and non-Abelian statistics in three dimensions, *Phys. Rev. Lett.* 104(4), 046401 (2010)
51. J. P. Xu, M. X. Wang, Z. L. Liu, J. F. Ge, X. Yang, C. Liu, Z. A. Xu, D. Guan, C. L. Gao, D. Qian, Y. Liu, Q. H. Wang, F. C. Zhang, Q. K. Xue, and J. F. Jia, Experimental detection of a Majorana mode in the core of a magnetic vortex inside a topological insulator-superconductor $Bi_2Te_3/NbSe_2$ heterostructure, *Phys. Rev. Lett.* 114(1), 017001 (2015)
52. H. H. Sun, K. W. Zhang, L. H. Hu, C. Li, G. Y. Wang, H. Y. Ma, Z. A. Xu, C. L. Gao, D. D. Guan, Y. Y. Li, C. Liu, D. Qian, Y. Zhou, L. Fu, S. C. Li, F. C. Zhang, and J. F. Jia, Majorana zero mode detected with spin selective andreev reflection in the vortex of a topological superconductor, *Phys. Rev. Lett.* 116(25), 257003 (2016)
53. F. Yang, Y. Ding, F. Qu, J. Shen, J. Chen, Z. Wei, Z. Ji, G. Liu, J. Fan, C. Yang, T. Xiang, and L. Lu, Proximity effect at superconducting Sn-Bi_2Se_3 interface, *Phys. Rev. B* 85, 104508 (2012)
54. G. Koren, T. Kirzhner, Y. Kalcheim, and O. Millo, Signature of proximity-induced p_x+ip_y triplet pairing in the doped topological insulator Bi_2Se_3 by the *s*-wave superconductor NbN, *Europhys. Lett.* (*EPL*) 103(6), 67010 (2013)
55. J. Wang, C. Z. Chang, H. Li, K. He, D. Zhang, M. Singh, X.C. Ma, N. Samarth, M. Xie, Q.K. Xue, and M. H. W. Chan, Interplay between topological insulators and superconductors, *Phys. Rev. B* 85, 045415 (2012)
56. S. Sasaki, M. Kriener, K. Segawa, K. Yada, Y. Tanaka, M. Sato, and Y. Ando, Topological Superconductivity in $Cu_xBi_2Se_3$, *Phys. Rev. Lett.* 107(21), 217001 (2011)
57. S. Sasaki, Z. Ren, A. A. Taskin, K. Segawa, L. Fu, and Y. Ando, Odd-parity pairing and topological superconductivity in a strongly spin–orbit coupled semiconductor, *Phys. Rev. Lett.* 109(21), 217004 (2012)
58. Q. L. He, H. Liu, M. He, Y. H. Lai, H. He, G. Wang, K. T. Law, R. Lortz, J. Wang, and I. K. Sou, Two-dimensional superconductivity at the interface of a Bi_2Te_3/FeTe heterostructure, *Nat. Commun.* 5(1), 4247 (2014)
59. P. Zareapour, A. Hayat, S. Y. Zhao, M. Kreshchuk, A. Jain, D. C. Kwok, N. Lee, S. W. Cheong, Z. Xu, A. Yang, G. D. Gu, S. Jia, R. J. Cava, and K. S. Burch, Proximity-induced high-temperature superconductivity in the topological insulators Bi_2Se_3 and Bi_2Te_3, *Nat. Commun.* 3(1), 1056 (2012)
60. M. Veldhorst, M. Snelder, M. Hoek, T. Gang, V. K. Guduru, X. L. Wang, U. Zeitler, W. G. van der Wiel, A. A. Golubov, H. Hilgenkamp, and A. Brinkman, Josephson supercurrent through a topological insulator surface state, *Nat. Mater.* 11(5), 417 (2012)

61. F. Qu, F. Yang, J. Shen, Y. Ding, J. Chen, Z. Ji, G. Liu, J. Fan, X. Jing, C. Yang, and L. Lu, Strong superconducting proximity effect in Pb-Bi_2Te_3 hybrid structures, *Sci. Rep.* 2(1), 339 (2012)
62. J. R. Williams, A. J. Bestwick, P. Gallagher, S. S. Hong, Y. Cui, A. S. Bleich, J. G. Analytis, I. R. Fisher, and D. Goldhaber-Gordon, Unconventional Josephson effect in hybrid superconductor–topological insulator devices, *Phys. Rev. Lett.* 109(5), 056803 (2012)
63. S. Hart, H. Ren, T. Wagner, P. Leubner, M. Mühlbauer, C. Brüne, H. Buhmann, L. W. Molenkamp, and A. Yacoby, Induced superconductivity in the quantum spin Hall edge, *Nat. Phys.* 10, 638 (2014)
64. E. Bocquillon, R. S. Deacon, J. Wiedenmann, P. Leubner, T. M. Klapwijk, C. Brune, K. Ishibashi, H. Buhmann, and L. W. Molenkamp, Gapless Andreev bound states in the quantum spin Hall insulator HgTe, *Nat. Nanotechnol.* 12(2), 137 (2016)
65. M. X. Wang, C. Liu, J. P. Xu, F. Yang, L. Miao, M. Y. Yao, C. L. Gao, C. Shen, X. Ma, X. Chen, Z. A. Xu, Y. Liu, S. C. Zhang, D. Qian, J. F. Jia, and Q. K. Xue, The coexistence of superconductivity and topological order in the Bi_2Se_3 thin films, *Science* 336(6077), 52 (2012)
66. S. Y. Xu, N. Alidoust, I. Belopolski, A. Richardella, C. Liu, M. Neupane, G. Bian, S. H. Huang, R. Sankar, C. Fang, B. Dellabetta, W. Dai, Q. Li, M. J. Gilbert, F. Chou, N. Samarth, and M. Z. Hasan, Momentum-space imaging of Cooper pairing in a half-Dirac-gas topological superconductor, *Nat. Phys.* 10(12), 943 (2014)
67. E. Wang, H. Ding, A. V. Fedorov, W. Yao, Z. Li, Y. F. Lv, K. Zhao, L. G. Zhang, Z. Xu, J. Schneeloch, R. Zhong, S. H. Ji, L. Wang, K. He, X. Ma, G. Gu, H. Yao, Q. K. Xue, X. Chen, and S. Zhou, Fully gapped topological surface states in Bi_2Se_3 films induced by a d-wave high-temperature superconductor, *Nat. Phys.* 9(10), 621 (2013)
68. Q. L. He, L. Pan, A. L. Stern, E. C. Burks, X. Che, G. Yin, J. Wang, B. Lian, Q. Zhou, E. S. Choi, K. Murata, X. Kou, Z. Chen, T. Nie, Q. Shao, Y. Fan, S. C. Zhang, K. Liu, J. Xia, and K. L. Wang, Chiral Majorana fermion modes in a quantum anomalous Hall insulator-superconductor structure, *Science* 357(6348), 294 (2017)
69. C. F. Pai, Switching by topological insulators, *Nat. Mater.* 17(9), 755 (2018)
70. J. Han, A. Richardella, S. A. Siddiqui, J. Finley, N. Samarth, and L. Liu, Room-temperature spin–orbit torque switching induced by a topological insulator, *Phys. Rev. Lett.* 119(7), 077702 (2017)
71. Y. Wang, D. Zhu, Y. Wu, Y. Yang, J. Yu, R. Ramaswamy, R. Mishra, S. Shi, M. Elyasi, K. L. Teo, Y. Wu, and H. Yang, Room temperature magnetization switching in topological insulator-ferromagnet heterostructures by spin–orbit torques, *Nat. Commun.* 8(1), 1364 (2017)
72. M. Dc, R. Grassi, J. Y. Chen, M. Jamali, D. Reifsnyder Hickey, D. Zhang, Z. Zhao, H. Li, P. Quarterman, Y. Lv, M. Li, A. Manchon, K. A. Mkhoyan, T. Low, and J. P. Wang, Room-temperature high spin–orbit torque due to quantum confinement in sputtered Bi_xSe_{1-x} films, *Nat. Mater.* 17(9), 800 (2018)
73. N. H. D. Khang, Y. Ueda, and P. N. Hai, A conductive topological insulator with large spin Hall effect for ultralow power spin–orbit torque switching, *Nat. Mater.* 17(9), 808 (2018)
74. D. A. Ivanov, Non-Abelian statistics of half-quantum vortices in p-wave superconductors, *Phys. Rev. Lett.* 86(2), 268 (2001)
75. J. Alicea, Y. Oreg, G. Refael, F. von Oppen, and M. P. A. Fisher, Non-Abelian statistics and topological quantum information processing in 1D wire networks, *Nat. Phys.* 7(5), 412 (2011)
76. D. Aasen, M. Hell, R. V. Mishmash, A. Higginbotham, J. Danon, M. Leijnse, T. S. Jespersen, J. A. Folk, C. M. Marcus, K. Flensberg, and J. Alicea, Milestones toward Majorana-based quantum computing, *Phys. Rev. X* 6 , 031016 (2016)
77. T. Karzig, C. Knapp, R. M. Lutchyn, P. Bonderson, M. B. Hastings, C. Nayak, J. Alicea, K. Flensberg, S. Plugge, Y. Oreg, C. M. Marcus, and M. H. Freedman, Scalable designs for quasiparticle-poisoning-protected topological quantum computation with Majorana zero modes, *Phys. Rev. B* 95(23), 235305 (2017)
78. J. Alicea, New directions in the pursuit of Majorana fermions in solid state systems, *Rep. Prog. Phys.* 75(7), 076501 (2012)
79. A. Y. Kitaev, Fault-tolerant quantum computation by anyons, *Ann. Phys.* 303(1), 2 (2003)
80. S. Hart, H. Ren, T. Wagner, P. Leubner, M. Mühlbauer, C. Brüne, H. Buhmann, L. W. Molenkamp, and A. Yacoby, Induced superconductivity in the quantum spin Hall edge, *Nat. Phys.* 10(9), 638 (2014)